Modeling and design of milled microwave printed circuit boards

Djordjevic, A.R.; Olcan, D.I.; Zajic, A.G.

Abstract available at: http://onlinelibrary.wiley.com/doi/10.1002/mop.25724/abstract

Article first published online: 15 DEC 2010

DOI: 10.1002/mop.25724

Issue
Microwave and Optical Technology Letters

Volume 53, Issue 2, pages 264–270, February 2011

device at 3–8 GHz [21]. The insertion loss for the BaM-PZT phase shifter is of the same order as for YIG-BST and YIG-PZT MSSW phase shifters [20, 21], but much higher than for YIG-PZT and YIG/PMN-PT/terfenol-D phase shifters [13, 15].

4. CONCLUSIONS

A mm-wave electric field tunable ferrite-piezoelectric phase shifter operating close to FMR is designed and characterized. The voltage tenability of the ferrite phase shifter is achieved through mechanical strain mediated magneto-electric effect in the bilayer. Differential phase shifts of 45° could be obtained with a nominal electric field of 8 kV/cm. The device shows an insertion loss >20 dB at 50 GHz. The electrical tuning will lead to integrated circuit-compatible high-speed phase shifters. Miniaturization of the device could be accomplished with the use of thin film magnets for the required bias magnetic field.

ACKNOWLEDGMENTS

This work was supported by grants from the Army Research Office and the Office of Naval Research.

REFERENCES

1. J.D. Adam, L.E. Davis, G.F. Dionne, E.F. Schloemann, and S.N. Stitzer, Ferrite devices and materials, IEEE Trans Microwave Theory Tech 50 (2002), 721–737.
2. N.I. Lyashenko, V.M. Talalaevsky, M.Y. Hvastuhin, and L.V. Chevnyuk, Influence of elastic pressure on spectra of magnetostatic waves in epitaxial YIG-films, Ukr J Phys 34 (1989), 1859–1860.
3. N.I. Lyashenko, V.M. Talalaevsky, and L.V. Chevnyuk, Influence of temperature and elastic pressure on dispersion characteristics of surface magnetostatic waves, Ukr J Phys 39 (1994), 1164–1169.
4. C.-W. Nan, M.I. Bichurin, S. Dong, D. Viehland, and G. Srinivasan, Multiferroic magnetoelectric composites: Historical perspective, status and future directions, J Appl Phys 103 (2008), 031101.
5. J. Zhai, Z. Xing, S. Dong, J. Li, and D. Viehland, Magnetoelectric laminate composites: An overview, J Am Ceram Soc 91 (2008), 351–358.
6. G. Srinivasan and Y.K. Fetisov, Microwave magnetoelectric effects and signal processing devices, Integr Ferroelectr 83 (2006), 89–98.
7. J. Lou, D. Reed, C. Pettiford, M. Liu, P. Han, S. Dong, and N.X. Sun, Giant microwave tunability in FeGaB/lead magnesium niobate-lead titanate multiferroic composite, Appl Phys Lett 92 (2008), 262502.
8. Y. Chen, J. Wang, M. Liu, N.X. Sun, C. Vittoria, and V. Harris, Giant magnetoelectric coupling and E-field tenability in a laminate Ni_2MnGa/PMN-PT multiferroic heterostructure, Appl Phys Lett 93 (2008), 112502.
9. C. Pettiford, J. Lou, L. Russell, and N.X. Sun, Strong magnetoelectric coupling at microwave frequencies in metallic magnetic film/lead zirconate titanate multiferroic composites, Appl Phys Lett 92 (2008), 122506.
10. J. Das, Y.Y. Song, N. Mo, P. Krivosik, and C.E. Patton, Electric-field-tunable low loss multiferroic ferrimagnetic-ferroelectric heterostructures, Adv Mater 21 (2009), 2045.
11. M.I. Bichurin, V.M. Petrov, Y.V. Kiliba, and G. Srinivasan, Magnetic and magnetoelectric susceptibility of a ferroelectric/ferromagnetic composite at microwave frequencies, Phys Rev B 66 (2002), 134404.
12. S. Shastry, G. Srinivasan, M.I. Bichurin, V.M. Petrov, and A.S. Tatarenko, Microwave magnetoelectric effects in single crystal bilayers of yttrium iron garnet and lead magnesium niobate-lead titanate, Phys Rev B 70 (2004), 064416.
13. A.S. Tatarenko, G. Srinivasan, and M.I. Bichurin, A magnetoelectric microwave phase shifter, Appl Phys Lett 88 (2006), 183507.
14. J. Lou, D. Reed, M. Liu, and N.X. Sun, Electrostatically tunable magnetoelectric inductors with large inductance tunability, Appl Phys Lett 94 (2009) 112508.
15. A.L. Geiler, S.M. Gillette, Y. Chen, J. Wang, Z. Chen, S.D. Yoon, P. He, J. Cao, C. Vittoria, and V.G. Harris, Multiferroic heterostructure fringe field tuning of meander line microstrip ferrite phase shifter, Appl Phys Lett 96 (2010), 053508.
16. G. Srinivasan, I.V. Zavislyak, and A.S. Tatarenko, Millimeter-wave magnetoelectric effects in bilayers of barium hexaferrite and lead zirconate titanate, Appl Phys Lett 89 (2006), 152508.
17. K.-H. Hellwege and A.M. Springer, (Eds.), Landolt-Bornstein: Numerical data and functional relationships in science and technology, Group III, Crystal and Solid State Physics, Vol. 4(b), Magnetic and Other Properties of Oxides, Springer-Verlag, New York, 1970.
18. L.E. Cross, Ferroelectric ceramics: Tailoring properties for specific applications, In: N. Setter (Ed.), Ferroelectric ceramics, Birkhäuser, Basel, 1993.
19. M.I. Bichurin, R.V. Petrov, and Y.V. Kiliba, Magnetoelectric microwave phase shifters, Ferroelectrics 204 (1997), 311–319.
20. Y.K. Fetisov and G. Srinivasan, A ferrite/piezoelectric microwave phase shifter: Studies on electric field tunability, Electron Lett 41 (2005), 1066–1067.
21. A. Ustinov, G. Srinivasan, and B.A. Kalinikos, Ferrite-ferroelectric hybrid wave phase shifters, Appl Phys Lett 90 (2007), 031913.

MODELING AND DESIGN OF MILLED MICROWAVE PRINTED CIRCUIT BOARDS

Antonije R. Djordjević,[1] Dragan I. Olćan,[1] and Alenka G. Zajić[2]

[1] School of Electrical Engineering, University of Belgrade, P.O. Box 35-54, 11120 Belgrade, Serbia; Corresponding author: olcan@etf.rs

[2] School of Computer Science, Georgia Institute of Technology, Atlanta, GA 30332

Received 15 May 2010

ABSTRACT: *This article investigates the influence of milling process on properties of printed microwave circuits. Furthermore, design guidelines are proposed for optimizing the milling process by leaving large unmilled copper surfaces on the board without deteriorating circuit performance. The proposed concepts are experimentally verified.* © 2010 Wiley Periodicals, Inc. Microwave Opt Technol Lett 53:264–270, 2011; View this article online at wileyonlinelibrary.com. DOI 10.1002/mop.25724

Key words: *printed circuit boards; milling process; transmission lines; parasitic resonances*

1. INTRODUCTION

Production of printed circuit boards (PCBs) using milling process enables fast production times, which is very convenient for prototyping. However, the milling process introduces certain peculiarities that may significantly affect the performance of microwave circuits.

First, the milling always makes grooves in the substrate. Furthermore, it may also create sloped copper sides, depending on the tool used for milling. Hence, the geometry of the cross-section of transmission lines and other printed features is significantly different compared with photoetched PCBs. Consequently, the characteristic impedances and propagation coefficients of transmission lines are changed, and the resonant frequencies of resonators are affected [1]. Adequate modeling of the geometry may be needed [1, 2] to obtain good match between computed and measured data.

Second, to optimize the milling process, i.e., to reduce the milling time and to increase the life span of tools, it may be

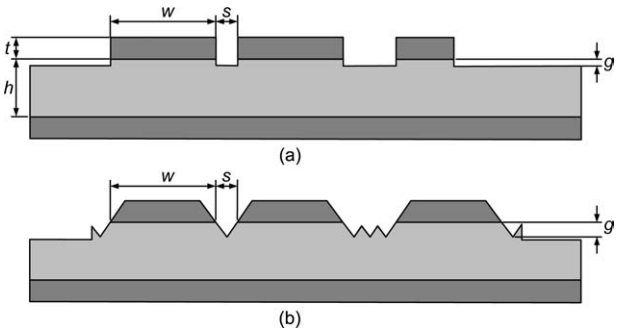

Figure 1 Typical profiles of machined PCB traces (cross-section) obtained with (a) cylindrical milling tool and (b) conical milling tool and cylindrical rubout tool

advantageous to keep copper surfaces intact as much as possible. Intact copper surfaces also enable better guiding of the milling tool, because rubbed-out portions of a surface may significantly lower the tool elevation. It is also desirable to reduce the number of vias, because they require additional processing. However, the unused copper surfaces (if they are not rubbed out) affect properties of transmission lines and other circuit elements. Worse than that, large floating copper surfaces (patches) create resonant structures with the ground plane, which can jeopardize circuit performance due to parasitic resonances [3].

The first objective of our article is to evaluate how typical cross-section profiles of milled structures (grooving the substrate and shaping the copper walls) affect properties of microwave circuits. In particular, we investigate how the milling process influences single and coupled transmission lines. The results show that if the characteristic impedance of a single transmission line is to be kept within tight limits, the strip width should be increased appropriately to compensate for the grooved dielectric. Our results also show that the groove depth affects the even impedance of the coupled transmission lines the same way as it impacts the characteristic impedance of a single transmission line. However, it has greater impact on the odd impedance of the coupled transmission lines. This is due to the capacitive coupling between the strips, which strongly depends on the dielectric located in the region between the strips. Finally, the results show that removing the dielectric reduces the dielectric losses. As the dielectric removal requires a wider trace to keep the characteristic impedance constant, the attenuation coefficient due to the conductor losses is also reduced.

The second objective of our article is to establish design guidelines for leaving large unmilled copper surfaces while minimizing their influence on the circuit performance. The results show that for frequencies below the first resonant frequency of the unmilled copper surfaces, the influence of these surfaces diminishes with increasing the width of the gap between the transmission line and the leftovers, as expected. Hence, to increase the resonant frequencies of leftovers above the operating band of the microwave circuit and thus passivize the copper areas, the copper leftover areas should be divided into smaller patches. (Smaller copper patches have larger resonant frequencies.) This can be easily achieved by using narrow grooves. Finally, to demonstrate the concepts developed in this article, a microstrip coupled resonator filter with two half wavelength edge-coupled resonators is designed, prototyped, and measured.

The remainder of the article is organized as follows. Section 2 investigates the influence of milling process on the properties of single and coupled transmission lines. Section 3 presents the design guidelines on how to minimize the influence of large unmilled copper surfaces on the circuit performance. Section 4 presents a design example of a microwave circuit produced by milling. Finally, Section 5 provides some concluding remarks.

2. CROSS-SECTION PROFILE

This section evaluates how typical cross-section profiles obtained by the milling process (i.e., grooving the substrate and shaping the copper walls) affect properties of microwave circuits. In particular, we investigate how the milling process affects the properties of single and coupled transmission lines.

While removing the copper, the milling tools also dig into the substrate to a certain depth (g), leaving a grooved surface (Fig. 1). The shape of the cross-section of microstrip traces (lines) produced by the milling process depends on the tool used. Some tools are effectively cylindrical and produce practically vertical walls of the copper traces (Fig. 1a). Other tools are conical and produce sloped walls of the copper traces (Fig. 1b).

The copper surface is somewhat uneven (both top and bottom), so that an increased tool depth is necessary to securely remove the copper. Furthermore, rubbing out unused copper surfaces is performed using a wide crude tool, which usually digs deeper into the substrate. However, being far away from the traces, the profile caused by the rubout tool usually has negligible influence on the properties of transmission lines and other components of the microwave circuit because the electromagnetic field is localized in the vicinity of the traces. Hence, the performance of microwave circuits is mainly affected by the shape of the conductors and dielectrics in the vicinity of the conductors. For example, the characteristic impedance of the microstrip line (Z_c) and the velocity of wave propagation (c) increase if the dielectric near the trace is grooved (i.e., the relative effective permittivity, $\varepsilon_{r,eff}$, decreases).

To illustrate how microwave circuits are affected by the shape of the conductors and dielectrics, Table 1 shows the variations of the characteristic impedance and effective relative permittivity versus the groove depth for a cylindrical tool and a conical tool. The total angle at the tip of the conical tool is 90°.

In all numerical and experimental examples in this article, we used the Rogers 4003 substrate, $h = 20$ mil (0.508 mm) thick, with $t = 35$ μm thick copper cladding. The nominal relative permittivity of the substrate at 10 GHz is 3.38 [4]. However, the manufacturer suggests using a higher value for the design. The value suggested in Ref. 4 is 3.55, whereas 3.55 for 60 mil thick substrates and 3.63 for 20 mil thick substrates are reported in Ref. 5. The measured value in Ref. 6 for an 8 mil thick substrate is 3.75. Our fit of experimental data for a 20 mil thick substrate yields a value of 3.7, which we have used in all computations. The substrate loss tangent is assumed to be 0.002

TABLE 1 Characteristic Impedance (Z_c) and Relative Effective Permittivity ($\varepsilon_{r,eff}$) of Microstrip Trace Versus Groove Depth (g), for Cylindrical and Conical Tools

	Cylindrical Tool		Conical Tool (90°)	
g (μm)	Z_c (Ω)	$\varepsilon_{r,eff}$	Z_c (Ω)	$\varepsilon_{r,eff}$
0	50.01	2.862	50.02	2.885
10	50.25	2.835	50.20	2.864
20	50.47	2.810	50.35	2.847
50	51.04	2.748	50.70	2.808
100	51.85	2.663	51.10	2.764
200	53.15	2.534	51.57	2.714

TABLE 2 Even-Mode Characteristic Impedance (Z_{ce}) and Relative Effective Permittivity ($\varepsilon_{re,eff}$) and Odd-Mode Characteristic Impedance (Z_{co}) and Relative Effective Permittivity ($\varepsilon_{ro,eff}$) for Two Coupled Microstrip Traces Versus Groove Depth (g), for Cylindrical and Conical Tools

	Cylindrical Tool		Conical Tool (90°)					
g (μm)	Z_{ce} (Ω)	$\varepsilon_{re,eff}$	Z_{co} (Ω)	$\varepsilon_{ro,eff}$	Z_{ce} (Ω)	$\varepsilon_{re,eff}$	Z_{co} (Ω)	$\varepsilon_{ro,eff}$
0	59.43	3.081	36.81	2.463	59.71	3.094	37.67	2.510
10	59.62	3.061	37.16	2.417	59.85	3.079	37.93	2.474
20	59.80	3.042	37.48	2.377	59.97	3.067	38.15	2.446
50	60.28	2.995	38.18	2.289	60.24	3.039	38.58	2.393
100	60.96	2.928	39.02	2.193	60.53	3.011	38.89	2.353
200	62.14	2.818	40.06	2.080	–	–	–	–

at 1 GHz. The effective surface roughness of the copper top surface was measured in Ref. 6 to be 1.2 μm. Our estimate is that the effective surface roughness is close to 2 μm, which agrees with the existence of dendrites shown in the photomicrograph in Ref. 7. At 1 GHz, this surface roughness effectively reduces the conductivity of copper from 58 to 23 MS/m.

The results shown in Table 1 are obtained using the 2D quasistatic analysis implemented in program Linpar [8]. It is assumed that the trace width (measured at the copper-to-substrate interface) is kept constant and equal to the trace width for an ideal 50-Ω trace ($w = 1.0836$ mm for the cylindrical tool and $w = 1.096$ mm for the conical tool).

From Table 1, we can observe that the cylindrical tool has greater influence on the transmission line properties. This is expected, because the cylindrical tool digs vertical walls in the substrate. To keep the error in the characteristic impedance less than 2%, the groove depth should not exceed 50 μm for the cylindrical tool and 80 μm for the conical tool.

We note that grooving the dielectric modifies the per-unit-length capacitance of the line (C'), but does not affect the per-unit-length inductance (L') because the dielectric properties of the environment do not affect the quasistatic inductance. As the characteristic impedance and the velocity (c) of wave propagation are related by $Z_c = cL'$, the relative increases of the velocity of wave propagation and of the characteristic impedance are identical. Hence, we can conclude that if the characteristic impedance is to be kept within tight limits, the strip width should be increased appropriately to compensate for the grooved dielectric.

The grooved dielectric also influences the coupling between adjacent lines. To illustrate this effect, Table 2 shows the even-mode and the odd-mode characteristic impedances and the relative effective permittivities for two symmetrical tightly coupled traces, versus the groove depth. The results are obtained using Linpar. The strip dimensions are same as for the single line from Table 1. The width of the gap between the strips is $s =$ 200 μm. The results show that the groove depth impacts the even impedance in the same way as it impacts the characteristic impedance of a single transmission line. On the other hand, it has greater impact on the odd impedance. This is due to the capacitive coupling between the lines, which is strongly affected by the dielectric in the region between the strips.

Finally, we analyze how the groove depth influences the attenuation coefficients. For fair comparison, the characteristic impedance of a single microstrip line should be kept constant when the groove depth is changed. The results, presented in Table 3, are obtained using Linpar. The results show that the attenuation coefficients due to conductor losses (α_c) and due to dielectric losses (α_d) decrease with increasing the groove depth. Removing the dielectric (in particular near the wedges, where the electric field is very strong) reduces the dielectric losses. It also requires a wider trace (to keep the characteristic impedance constant), which, in turn, reduces the attenuation coefficient due to the conductor losses. Finally, we can observe that the sharp copper wedges produced by the conical tool increase the conductor losses due to the larger concentration of current at the wedges (compared with the right-angle wedges produced by the cylindrical tool). Similar reasoning is given in Ref. 1, but the strip width was kept constant in that paper. In addition, the hybrid nature of the propagating wave was pronounced in Ref. 1 due to the high operating frequency, unlike in our case, where we can still assume the quasi-TEM wave propagation.

3. COPPER LEFTOVERS

To reduce the milling time and reduce tool wear out, it is desirable to leave copper surfaces intact as much as possible. This section presents some design guidelines on how to minimize the influence of large unmilled copper surfaces on the circuit performance.

To illustrate how the copper leftovers impact the circuit performance, we analyze a microstrip trace shown in Figure 2. The trace is defined by milling two slots around it, while leaving the

TABLE 3 Adjusted Strip Width (w) for 50-Ω Line, Relative Effective Permittivity ($\varepsilon_{r,eff}$), Attenuation Coefficient Due To Conductor Losses (α_c), and Attenuation Coefficient Due To Dielectric Losses (α_d) at 1 GHz Versus Groove Depth (g), For the Cylindrical and Conical Tools

	Cylindrical Tool		Conical Tool					
g (μm)	w (mm)	$\varepsilon_{r,eff}$	α_c (Np/m)	α_d (Np/m)	w (mm)	$\varepsilon_{r,eff}$	α_c (Np/m)	α_d (Np/m)
0	1.083	2.862	0.1262	0.0310	1.096	2.885	0.1345	0.0314
10	1.093	2.837	0.1254	0.0307	1.103	2.866	0.1339	0.0311
20	1.100	2.815	0.1248	0.0303	1.108	2.850	0.1334	0.0309
50	1.120	2.759	0.1232	0.0295	1.120	2.815	0.1323	0.0305
100	1.147	2.685	0.1210	0.0286	1.135	2.776	0.1311	0.0300
200	1.189	2.576	0.1178	0.0271	1.150	2.731	0.1297	0.0296

Figure 2 Microstrip trace surrounded by large floating copper areas

remaining large copper areas intact. To avoid vias (which require extra drilling and further processing), the copper leftovers are left floating.

There are two distinct influences of the copper leftovers on the circuit performance. The first influence is broadband, and the second influence is resonant.

The broadband influence is the dominant effect at lower frequencies, before the resonances occur. Due to the large capacitance between a leftover copper patch and the ground (Fig. 2), the patch practically behaves as if it is grounded. Hence, the structure shown in Figure 2 resembles a grounded coplanar waveguide (GCPW). (A coplanar waveguide is actually a transmission line, not a waveguide. A more proper name for this line is ''coplanar transmission line'' [9], although this term is not widely recognized.) The characteristic impedance of the microstrip line is affected by the presence of the two large copper wings. To illustrate this effect, Figure 3 shows the apparent characteristic impedance of the microstrip trace versus the gap width. The microstrip trace is $w = 1.083$ mm wide and surrounded by two copper patches that are $d = 20$ mm wide. The results are obtained by modeling the structure as three coupled microstrip lines using program MWO [10], whose kernel analyzes transmission lines following the same procedure as in Ref. 8. The characteristic impedance of a line simulated in MWO is found by optimizing the port nominal impedances with the goal of obtaining the lowest possible reflection. For comparison, Figure 3 also shows the characteristic impedance of a GCPW obtained with Linpar. We can observe that the two curves are very close. We observed that the resemblance increases with increasing the copper patch width (d in Fig. 2). Figure 3 shows that, for a 50-Ω line, the influence of the neighboring copper patches on the characteristic impedance is 6% when the gap width is $s = h$. For $s = 2h$, the influence decreases to below 2%. In general, the influence of the copper leftovers diminishes with increasing the width of the gap between the middle trace and the leftovers. Furthermore, for a given width of the middle trace, the characteristic impedance is lower for the GCPW structure than for the classical microstrip line. Hence, to obtain a 50-Ω line, the width of the middle trace must be smaller than that for the classical microstrip line.

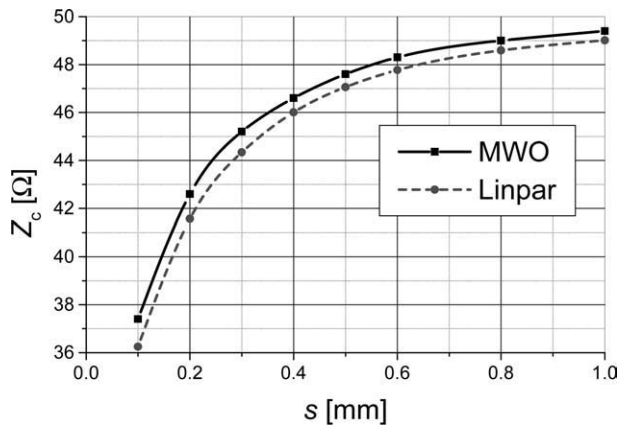

Figure 3 Characteristic impedance of microstrip trace shown in Figure 2 (Z_c) versus gap width (s)

The resonant influence is the dominant effect when the dimensions of the large intact copper area (a patch) become electrically large. The patch and the ground plane form a resonator. The lowest resonant frequency occurs when the largest patch dimension is approximately equal to the half wavelength (measured in the substrate). In the vicinity of the resonant frequencies, the copper leftovers can significantly impair the circuit performance, in particular if the coupling is strong. At resonances, the electromagnetic compatibility performance of the circuit is also deteriorated, because a resonant patch behaves like a microstrip antenna, and it can significantly radiate.

To illustrate the resonant effect, Figure 4 shows the scattering parameter s_{21} of the microstrip trace shown in Figure 2 for

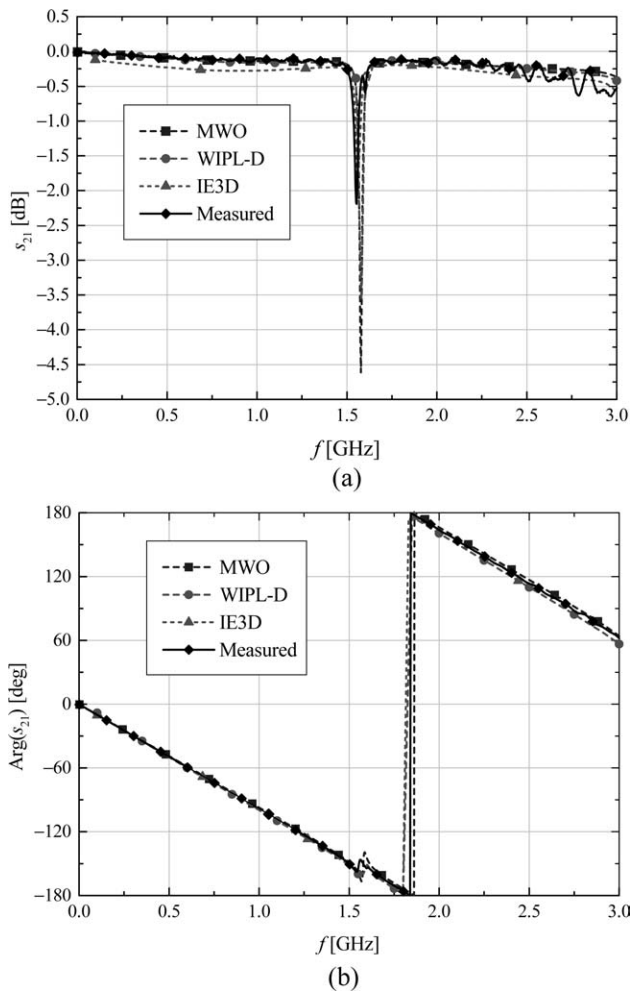

Figure 4 (a) Magnitude and (b) phase of the transmission scattering parameter of the microstrip trace obtained by experiment and by computer simulation using various models

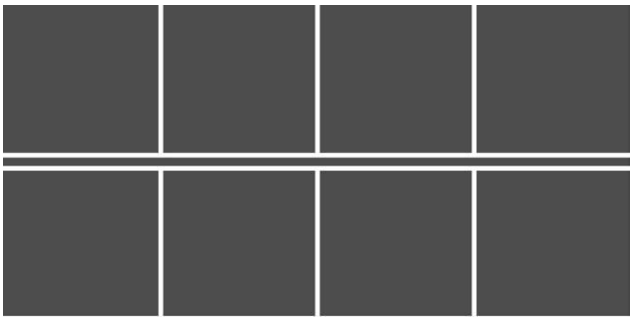

Figure 5 Microstrip trace surrounded by large copper areas that are divided into smaller patches

$w = 0.7$ mm, $s = s = 0.28$ mm, $d = 12$ mm, and the line length $l = 50$ mm. The curves in Figure 4 are obtained experimentally as well as using various simulation models. Milling was performed using a high-precision MITS milling machine with 50 μm line/space resolution [11]. Measurements of the scattering parameters were performed using Agilent E5062A network analyzer [12].

The first simulation model used to obtain the results in Figure 4 is the transmission line model (based on coupled microstrip lines in MWO). The model is very simple and fast, and the corresponding results are in remarkably good agreement with the experiment. The second model is a 3D model of arbitrary metallic and dielectric structures implemented in WIPL-D [13, 14], which can simulate arbitrary 3D metallic and dielectric structures with linear isotropic and piecewise homogeneous materials, based on solving integral equations for the equivalent surface sources using the method of moments [15]. The third model is a 3D model of layered structures implemented in IE3D [16], which is based on the Sommerfeld formulation.

The two wide microstrip traces (i.e., the large intact copper areas) are open at both ends. Hence, they represent resonators with the lowest resonant frequency at about 1.58 GHz. These resonators are relatively strongly coupled to the middle trace. The coupling is particularly strong at the resonant frequencies due to different modal velocities of propagation [17]. Note that if the dielectric is homogeneous, e.g., a vacuum, the patches are decoupled at the resonant frequency. Hence, the resonance cannot be seen in the transmission line model, although in reality there exists a very narrow resonance.

The influence of the resonances slowly diminishes when the distance between the copper patches and the microwave circuit is increased. However, to obtain negligible effects, the distance should be increased even beyond $10h$. This, in turn, requires rubbing out a large clearance between the circuit and the leftovers, thus annihilating the rationale for leaving large intact copper areas.

A better technical solution is to increase the resonant frequencies above the operating band of the microwave circuit, and thus passivize the copper leftover areas. This can be achieved by dividing the copper areas into smaller patches, by using narrow grooves. The passivization can be achieved with only a few grooves, which can be cut quickly, even using the same milling tool as for the basic microwave circuit. This procedure saves time, tool wear out, and the amount of debris. To illustrate this procedure, Figure 5 shows the layout of a transmission line where the large copper patches are divided into eight smaller patches. The resulting scattering parameters are shown in Figure 6. We can observe that the lowest parasitic resonance is shifted outside of the 0–3 GHz range.

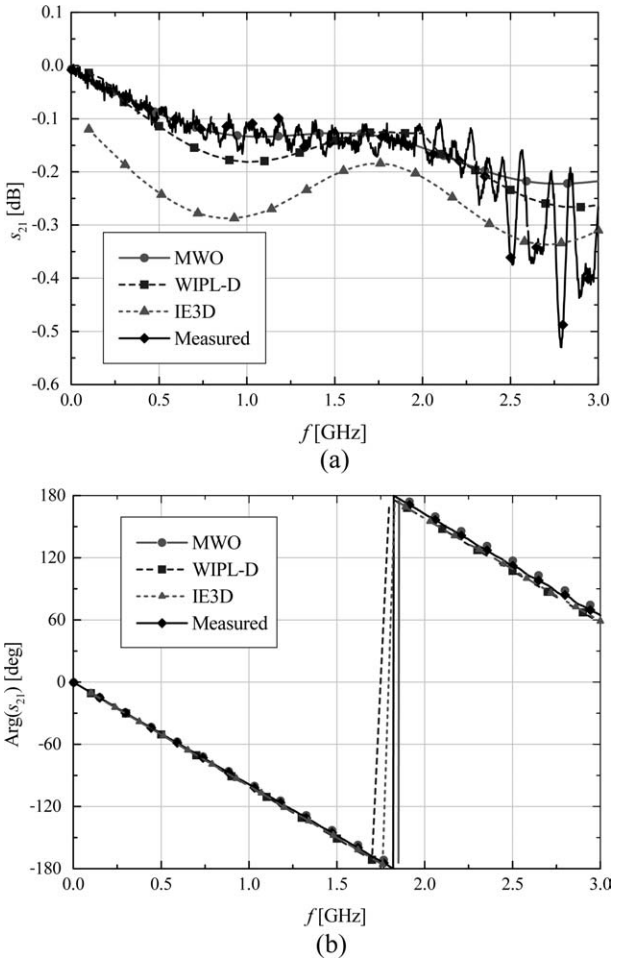

Figure 6 (a) Magnitude and (b) phase of the transmission scattering parameter of the microstrip trace shown in Figure 5 obtained by experiment and by computer simulation using various models

Note that the transmission line model can only predict resonant modes that correspond to waves whose direction of propagation is along the central microstrip line. The 3D solvers can also predict transverse resonances.

To verify the existence of the transverse resonances, we consider three different patch widths, w_p (Fig. 7). In all cases, we assume that the patches are congruent. The lengths of all

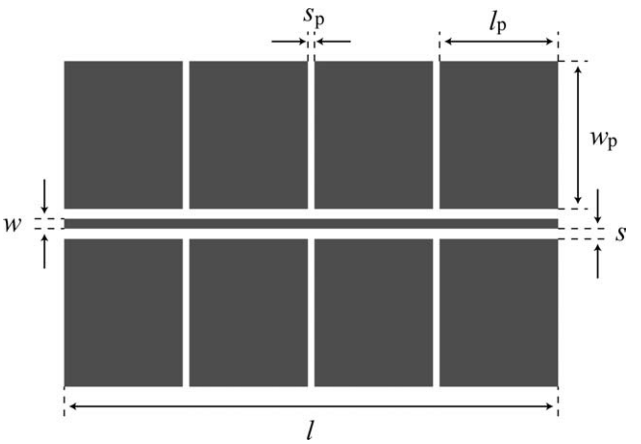

Figure 7 Microstrip trace surrounded by large copper areas that are divided into smaller patches

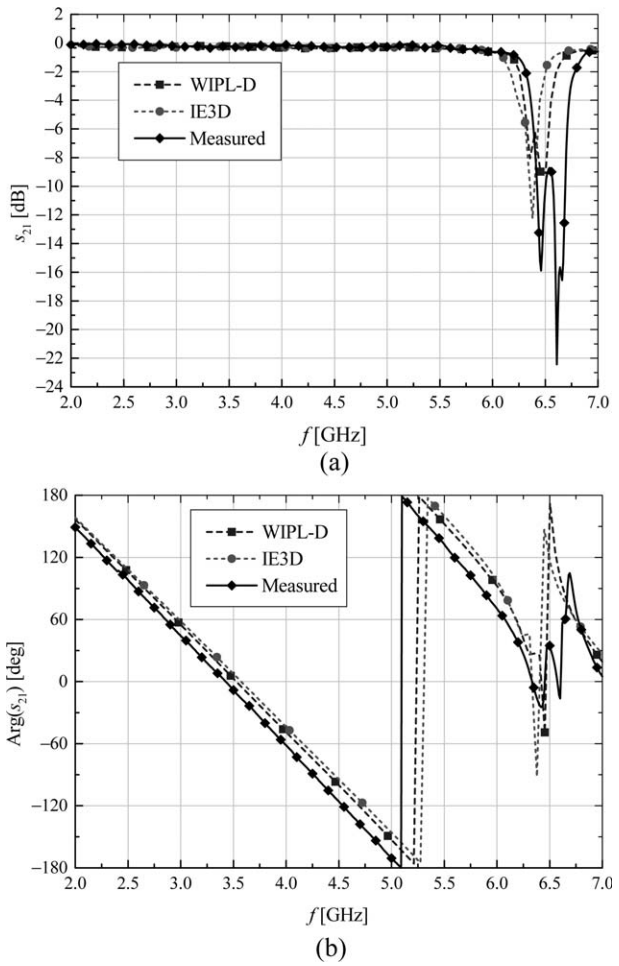

Figure 8 (a) Magnitude and (b) phase of the transmission scattering parameter for the line shown in Figure 7 for $w_p = 12$ mm

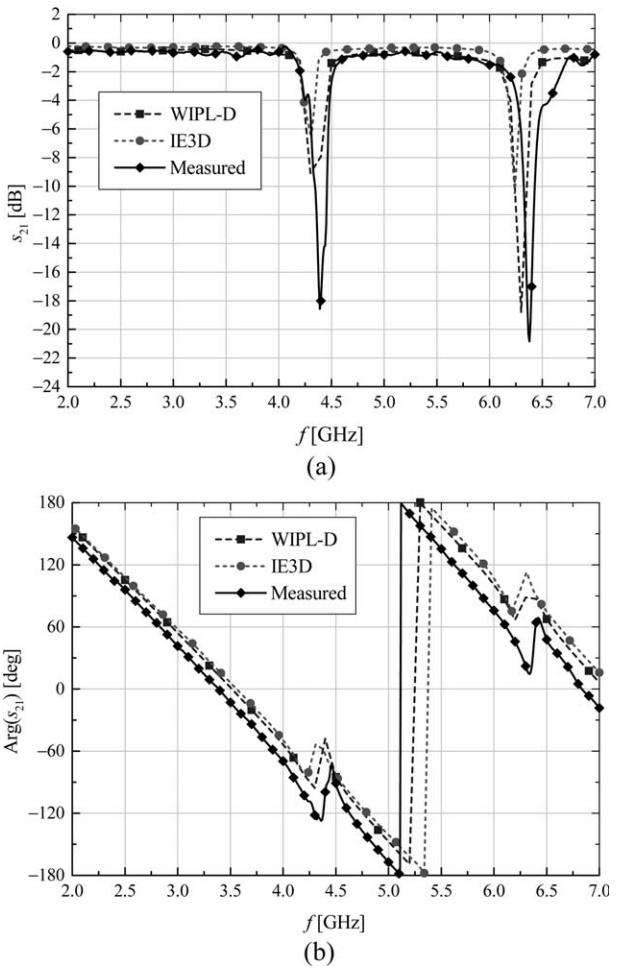

Figure 9 (a) Magnitude and (b) phase of the transmission scattering parameter for the line shown in Figure 7 for $w_p = 18$ mm

patches are $l_p = 12$ mm. In all three cases, the width of the microstrip trace is $w = 0.7$ mm, and the length is $l = 50$ mm. The gap between any two neighboring patches is $s_p = 0.67$ mm. The gap between the patches and the microstrip trace is $s = 0.28$ mm. Scattering parameters of the microstrip trace are evaluated using programs WIPL-D and IE3D. The traces are fabricated and measured. The simulation and measurement results for the parameter s_{21} are shown in Figures 8–10. F8-F10

For $w_p = 12$ mm, both models show a resonance at 6.35 GHz (Fig. 8). Note that at the resonant frequency, both w_p and l_p are close to half wavelength (in the substrate). For $w_p = 18$ mm (Fig. 9), the simulation shows two resonances in the range 2–7 GHz. The first resonance is at 4.3 GHz, where w_p is half

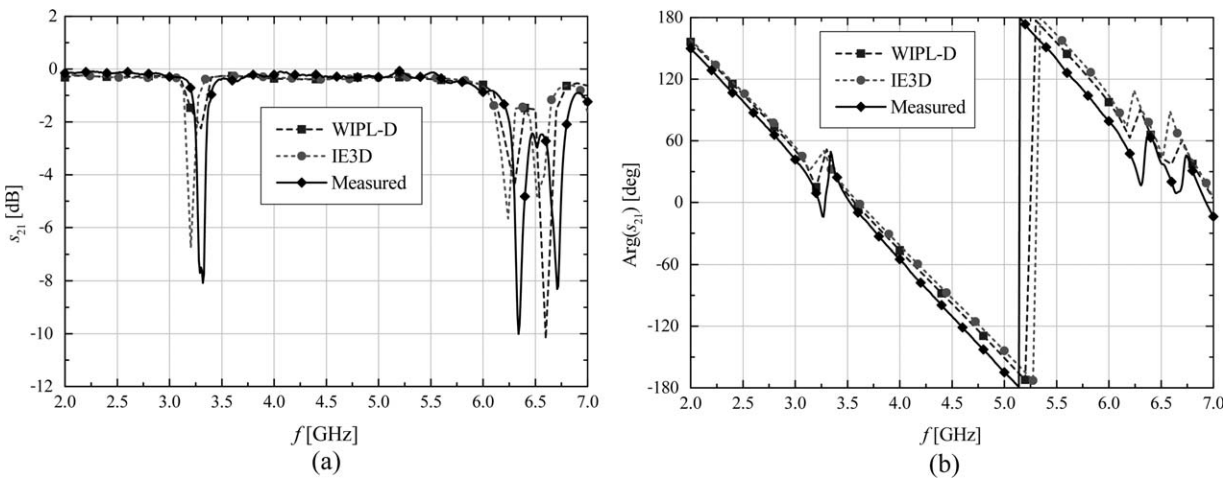

Figure 10 (a) Magnitude and (b) phase of the transmission scattering parameter for the line shown in Figure 7 for $w_p = 24$ mm

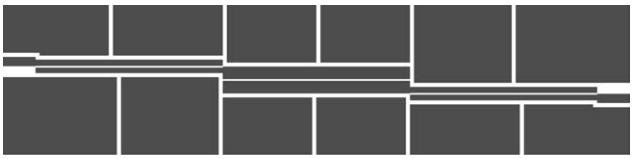

Figure 11 Layout of coupled resonator filter with passivized copper leftovers

wavelength. The second resonance is at 6.35 GHz, where l_p is half wavelength. Finally, for $w_p = 24$ mm (Fig. 10), the first resonant frequency is 3.2 GHz, where w_p is half wavelength, and the second resonant frequency is 6.35 GHz. In all cases, the resonant frequencies obtained from the computer simulation agree very well with the measurements. It can be concluded from these results that the largest dimension of the patch always determines the lowest resonant frequency. To keep the first resonant frequency safely above the operating band of the circuit, the largest patch dimension should be sufficiently smaller than the half wavelength at upper frequency limit of the band.

4. DESIGN EXAMPLE

This section shows a design example of a microwave circuit produced by milling, while leaving large copper patches on the board. We design a microstrip coupled resonator bandpass filter (centered at 2 GHz) with two half wavelength edge-coupled resonators, as shown in Figure 11. The gaps between the coupled microstrip lines are very narrow ($s = 80$ μm), although the copper thickness is substantial ($t = 35$ μm). Figure 12 shows the measured and simulated scattering parameters (using MWO), which show remarkably good agreement. The filter is surrounded by large copper patches. The first resonance of a patch is defined by its length. The largest patch length is $l_p = 14$ mm, which is about one-fifth of the wavelength (in the substrate) at the filter central frequency. Hence, the parasitic resonances are above 5.6 GHz, i.e., high above the filter passband, and their influence on the filter performance is negligible, which validates the design rule from Section 3.

5. CONCLUSIONS

This article investigates the influence of milling process on the properties of printed microwave circuits. In particular, we investigate how the milling process affects the properties of single and coupled transmission lines. Although the results presented in this article are not directly scalable to other substrate permittivities and thicknesses, they show the expectancies for the behavior of transmission lines and other circuit elements when produced by milling.

We also propose design guidelines for leaving large unmilled copper surfaces without deteriorating the circuit performance, thus optimizing the milling process. To demonstrate the concepts developed in this article, a microstrip coupled resonator filter with two half wavelength edge-coupled resonators is designed and prototyped. The measured and simulated results show remarkably good agreement.

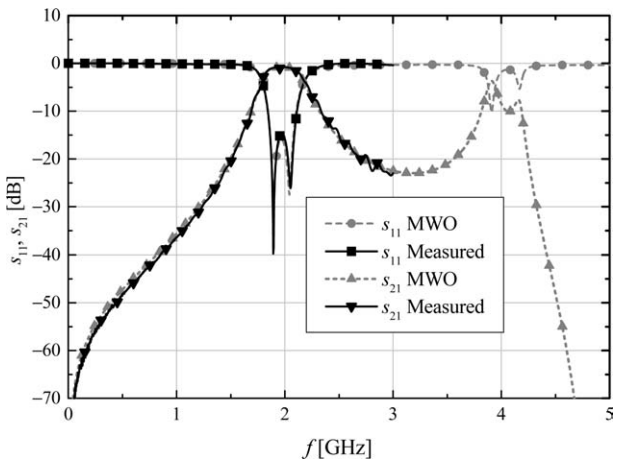

Figure 12 Magnitude of scattering parameters of the filter shown in Figure 11 obtained by experiment and computer simulation using MWO

ACKNOWLEDGMENTS

This work was supported by the Serbian Ministry of Science and Technological Development under grant TR 11021 and by the COST action IC0603.

REFERENCES

1. M. Gatchev, S. Kamenopolsky, V. Bojanov, and P. Dankov, Influence of the milling depth on the microstrip parameters in milled PCB-plates for microwave applications, Proc. of 14th Int. Conf. on Microwaves, Radar and Wireless Communications, vol. 2, 2002, pp. 476–479.
2. M. Helal, J.F. Legier, P. Pribetich, and P. Kennis, Analysis of planar transmission lines and microshield lines with arbitrary metallization cross sections using finite elements methods, IEEE MTT-S Digest, San Diego, CA, 1994, pp. 1041–1044.
3. A. Djordjević and Z. Maričević, Internal EM problems caused by parasitic resonances, IEEE International Symposium on Electromagnetic Compatibility, Washington, DC, 2000.
4. http://www.rogerscorp.com/documents/726/acm/RO4000-laminates-data-sheet-and-fabrication-guidelines-RO4003C-RO4350B.aspx
5. Rogers Corporation, Technical Report 6006, March 2006.
6. D. Marković, B. Jokanović, M. Marjanović, and M. Djordjević, Improved method for measurement of the dielectric properties of microwave substrates using microstrip T-resonator, Instrumentation and Measurement Technology Conference, Warsaw, Poland, 2007.
7. www.taconic-add.com/pdf/technicalarticles–DesignCon_2008_ATE_PCB_Materials.pdf
8. A.R. Djordjević, M.B. Baždar, R.F. Harrington, and T.K. Sarkar, LINPAR for windows: Matrix parameters for multiconductor transmission lines, Artech House, Norwood, MA, 1999.
9. R.E. Collin, Foundations for microwave engineering, Wiley, Hoboken, NY, 2001.
10. Microwave Office, Applied Wave Research, El Segundo, CA, 2002.
11. http://www.mitspcb.com/edoc/fp21t_p.htm
12. http://www.home.agilent.com/agilent/product.jspx?nid=536902639.536883619.00&cc=US&lc=eng
13. B.M. Kolundžija, J.S. Ognjanović, T.K. Sarkar, D.S. Šumić, M.M. Paramentić, B.B. Janić, D.I. Olćan, D.V. Tošić, and M.S. Tasić, WIPL-D microwave software and user's manual, WIPL-D/Artech House, Belgrade/Norwood, MA, 2005.
14. WIPL-D Pro v6.4, Software and user's manual, WIPL-D d.o.o., Belgrade, 2008. Available at: www.wipl-d.com.
15. R.F. Harrington, Field computation by moment methods, Macmillan, New York, 1968; Reprinted by IEEE Press, New York, 1993.
16. IE3D v9, Zeland Software, Inc. Fremont, CA. 2003. Available at: http://www.zeland.com.
17. A.R. Djordjević, T.K. Sarkar, and R.F. Harrington, Time-domain response of multiconductor transmission lines, Proc IEEE 75 (1987), 743–764.